

# An Outdoor Multipath Channel Model for Vehicular Visible Light Communication Systems

Hasan Farahneh<sup>1\*</sup> , Dia I. Abualnadi<sup>2</sup> 

<sup>1,2</sup>Electrical Engineering Department, School of Engineering, The University of Jordan, Amman, Jordan

E-mail: h.farahneh@ju.edu.jo

Received: October 10, 2021

Revised: November 22, 2021

Accepted: November 27, 2021

**Abstract**— Visible light communication is increasingly getting attention as a promising candidate to provide vehicle-to-vehicle communications. In this paper, we develop an accurate channel model for an outdoor optical wireless propagation scenario from the fundamental principles. General number of transmitting elements, reflectors and receiving elements are considered which essentially reflect a multipath multiple input multiple output (MIMO) optical wireless channel. Derived impulse response function is used to evaluate the channel and its fading characteristics. The channel model is also evaluated using an on-off-keying communication link with maximum likelihood detection. An expression for the probability density function at the receiver is derived considering multipath effects as well as background radiation noise. Simulation results show the dependency of the channel gain on the transmitter receiver field of views and the number of reflections. In general, this channel model can be used to evaluate optical wireless communication systems.

**Keywords**— Vehicle-to-vehicle communication; Visible light communication; Multipath fading; Signal detection; Bit error rate; Mobile communication; Wireless communications.

## 1. INTRODUCTION

As a relatively new technology, visible light communication (VLC) systems have gained greater attention in recent years in both academia and industry. This is primarily due to the accelerated developments of high-intensity light-emitting diode (LED) devices. For example, the luminous efficiency of current commercial white LEDs have increased to 10 times that of tungsten incandescent lamps [1]. LEDs are robust and also proven to have superior reliability and small form factor [2]. These properties have made them the de-facto standard for use in the automotive industry.

As an added bonus, LEDs can also be used in visible light data communications due to their faster rise time and high speed switching capabilities [3]. Vehicle-to-vehicle (V2V) VLC has great potential to be used in road safety applications. In June 2021, The World Health Organization (WHO) records conclude that every year the lives of approximately 1.3 million people are cut short as a result of road traffic crashes. Between 20 and 50 million more people suffer non-fatal injuries, with many incurring a disability as a result of their injury [4]. Furthermore, the number of vehicles and drivers are increasing yearly; thereby demanding increased safety measures. This can be achieved by an intelligent and reliable communication system for vehicles on the road. VLC is a great candidate in this application because most V2V communication is short range and line of sight (LOS). In addition, the polarization characteristic of visible light - if controlled appropriately - brings another degree of freedom that can multiply the transmission capacity [5].

VLC technology utilizes the wavelength band from 390 to 750 nm and has many advantages over radio frequency (RF) based communication technology employed for intelligent transportation system (ITS) applications. VLC has low complexity and

\* Corresponding author

implementation cost, especially since LED lamps are already installed in vehicles, traffic lights and street lights. Since LEDs exhibit highly directional LOS propagation characteristics, high accuracy positioning can be achieved. VLC based positioning technology can reduce the positioning error to tens of centimeters, which is more accurate than RF based positioning technology [6]. An RF based system experiences undesirable packet collisions and longer delays as well as poor packet reception rate during high demand hours, or during an increased vehicle density since RF signal propagation is unconfined. However, VLC technology can alleviate this limitation due to its directional propagation that limits receiving signals only from neighboring vehicles. This will effectively have impact on the safety, as well as reducing signal jamming [7, 8].

However, accurate VLC channel models are necessary for better system design. Modeling an outdoor V2V channel is a difficult task due to widely varying propagation characteristics that depend on meteorological conditions, mobility, scatterers, etc. In the literature, most of the optical wireless work is focused on indoor channel modeling, while there is little work on outdoor multipath mobile V2V channel for the VLC systems. In [9], authors introduced a new model for V2V communication system using visible light technology, while in [10], authors presented a hybrid modulation schemes for data transmission improvement for the VLC system. In [11], authors discussed and proposed a new method to overcome the effect of sunlight irradiance in VLC links used for V2V communication. They proposed K-Nearest Neighbor (KNN), a machine learning-based adaptive filter, to combat the effects of solar irradiance. The authors in [12] introduced VLC for inexpensive V2V using off the shelf LEDs and photo diodes (PDs). Although there are quite a few researches in the field of outdoor VLC application, the majority of research focuses on the indoor VLC applications for many challenges as will be mentioned briefly. It's a well-known fact that 47% of the total solar irradiance falls within the visible light frequency band of the spectrum. The main meteorological conditions in network locations determine the level of sunlight. Therefore, the major challenge of the outdoor VLC system is the strong influence of the ambient-light noise because of sunlight. Sunlight represents unmodulated sources, that can be received at an average power much larger than the desired signal, even when optical filtering is employed. However, the noise due to the solar irradiance and other surrounding light sources, is a major concern that degrades the performance of the VLC system in outdoor application in terms of signal to noise ratio (SNR) and bit error rate (BER). Also, due to the nature of the visible light spectrum, shadowing is a significant issue especially over short distances and small field of views (FOVs). This can seriously impair communications in both quasi-stationary indoor and fast varying outdoor V2V environments. However, by employing transmitters with a wide FOV as well as effectively utilizing the diffraction phenomenon of the light, the issues caused by shadowing can be alleviated. Note it is much better to implement diffuse transmitters which radiate the light over a wide solid angle, which does not have as severe pointing and shadowing problems when compared to point-to-point links. The diffused transmitter does not need to be aimed directly at the receiver since the radiated optical waves reflect from multiple surfaces.

In this paper, we derive an accurate closed form expression for the VLC channel in outdoor conditions considering multiple transmitters, multiple receivers and multiple reflectors (MIMO VLC). We also consider the polarization change in each reflection. An

expression for the impulse response is derived which completely describes the MIMO VLC channel with its multipath effects. We consider on-off-keying (OOK) intensity modulation at the transmitter and direct detection at the receiver side including photo detector noise variance. OOK modulation scheme is considered in this work because its modulation has already standardized for transmission of data in VLC technology. Also, it was observed that OOK outperformed the frequency-shift keying (FSK) modulation in terms of cost, BER and the simplicity of the circuit. This actually shows that by making use of OOK modulation in VLC, one can save money and can transmit information efficiently [13]. Simulation using different channel parameters reveals useful insight as shown in Table 1.

The rest of this paper is organized as follows: section 2 discusses the channel model, then in section 3, the complete channel response has been derived, where in section 4, signal detection has been discussed as well as a multipath mitigation technique. Section 5 provides final simulation results using Matlab<sup>TM</sup> and a final analysis of our results and models are provided in section 6.

## 2. CHANNEL MODEL

There has been very limited research on mobile VLC especially in vehicular applications. Our proposed topic provides a novel unified approach applied to the environment shown in Fig. 1. The communication between two vehicles can be considered as a MIMO model.

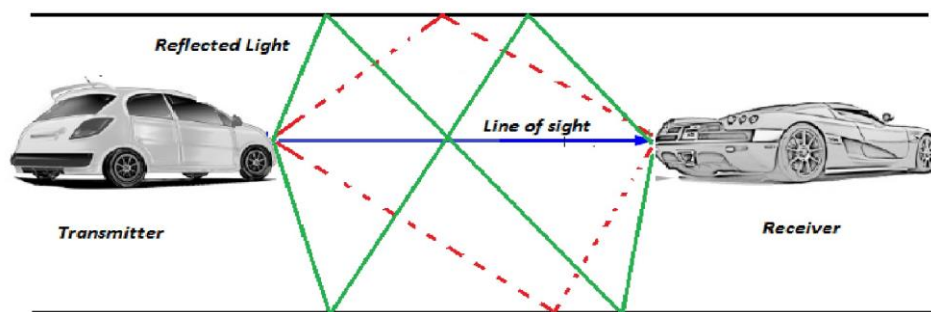


Fig. 1. VLC V2V communication link with multipath components.

Hence, the channel can be decomposed into various transfer matrices relevant to the V2V VLC environment. The authors in [14] derived an expression for the indoor channel but assumed each reflector to be of equal area. Moreover, they did not consider light polarization, as light undergoes polarization shifts when it is reflected on a surface. In this work, we adopt the same approach and modify it for outdoor applications. However, we assume the areas of the different reflectors to be unequal; also, we consider polarization alterations for VLC due to reflections. Note that transfer function between any two points can be decomposed into four essential components. Suppose there are  $J$  number of sources,  $N$  reflecting surface elements and  $M$  number of receivers; then, the four components are: the transfer function between a source and reflectors  $F_{J \times N}$ ; the transfer function between reflectors  $\phi_{N \times N}$ ; the transfer function between reflector and the receiver  $G_{N \times M}$ ; and the direct transfer function between source and receiver  $D_{J \times M}$ . This scenario is depicted in Fig. 2.

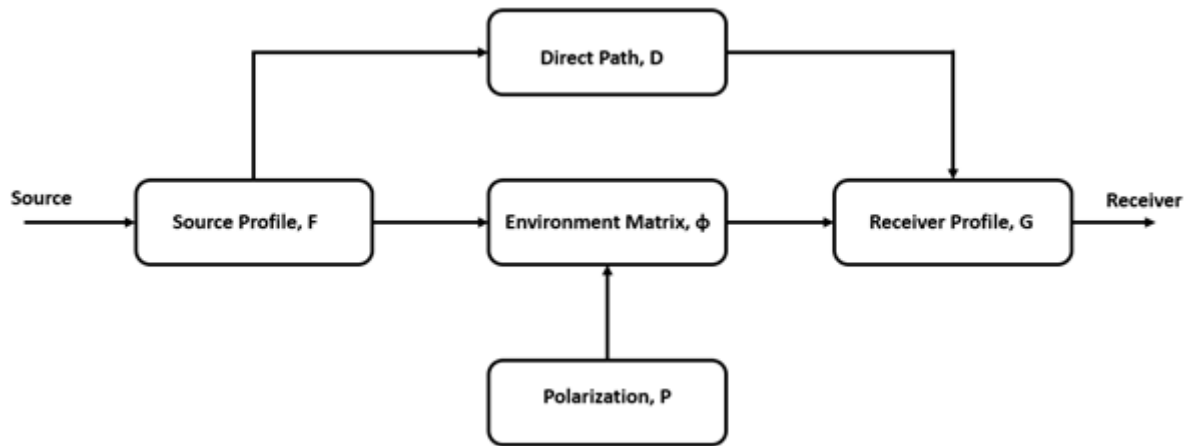


Fig. 2. Block diagram of V2V VLC channel.

### 2.1. Source Profile: $F_{J \times N}$

$$F_{J \times N} = \begin{bmatrix} f_{11} & f_{12} & \dots & f_{1N} \\ f_{21} & f_{22} & \dots & f_{2N} \\ \vdots & \vdots & \ddots & \vdots \\ f_{J1} & f_{J2} & \dots & f_{JN} \end{bmatrix}$$

Each entry of the matrix  $f_{sk}$  is the transfer function between a source  $s$  and element  $k$  and can be written as [9]:

$$f_{sk} = \frac{\left(\frac{n+1}{2\pi}\right) \cos^n(\phi_{sk}) \cos(\theta_{sk}) A_k}{R_{sk}^2} \delta\left(t - \frac{R_{sk}}{c}\right) u\left(\frac{\pi}{2} - \theta_{sk}\right) \quad (1)$$

where  $n$  is the Lambertian order of the source,  $\phi_{sk}$  is the emitting angle from source  $s$  to element  $k$ ,  $\theta_{sk}$  is the incident angle from source  $s$  to element  $k$ ,  $R_{sk}$  is the distance between source  $s$  and element  $k$ ,  $A_k$  is the area of the element  $k$ ,  $c$  is speed of light, and  $u(\cdot)$  is the unit step function.

### 2.2. Environment Matrix: $\Phi_{N \times N}$

The transfer function between reflectors  $\Phi_{N \times N}$  is an  $N$  by  $N$  matrix. Considering up to  $n$  reflections, it is expressed in matrix form as [9]:

$$\Phi_{N \times N} = \begin{cases} I_{N \times N} + \Psi_{N \times N} + \Psi_{N \times N}^2 + \dots + \Psi_{N \times N}^{n-1} & n \geq 2 \\ I_{N \times N} & n = 1 \end{cases}$$

where  $I_{N \times N}$  is the  $N$  by  $N$  identity matrix and  $\Psi_{N \times N}$  is given by [9]:

$$\Psi_{N \times N} = \begin{bmatrix} \psi_{11} & \psi_{12} & \dots & \psi_{1N} \\ \psi_{21} & \psi_{22} & \dots & \psi_{2N} \\ \vdots & \vdots & \ddots & \vdots \\ \psi_{N1} & \psi_{N2} & \dots & \psi_{NN} \end{bmatrix}$$

Here,  $\psi_{ik}$  represents the transfer function between two reflecting elements  $i$  and  $k$  and is stated as [9]:

$$\psi_{ik} = \begin{cases} 0 & i = k \\ \frac{\rho_i \cos(\phi_{ik}) \cos(\theta_{ik}) A_k}{\pi R_{ik}^2} \delta\left(t - \frac{R_{ik}}{c}\right) u\left(\frac{\pi}{2} - \theta_{ik}\right) & i \neq k \end{cases}$$

where  $\rho_i$  is the reflection coefficient of element  $i$ ,  $\phi_{ik}$  is the emitting angle from element  $i$  to element  $k$ ,  $\theta_{ik}$  is the incident angle from element  $i$  to element  $k$  and  $R_{ik}$  is the distance between element  $i$  and element  $k$ . This is clarified in Fig. 3.

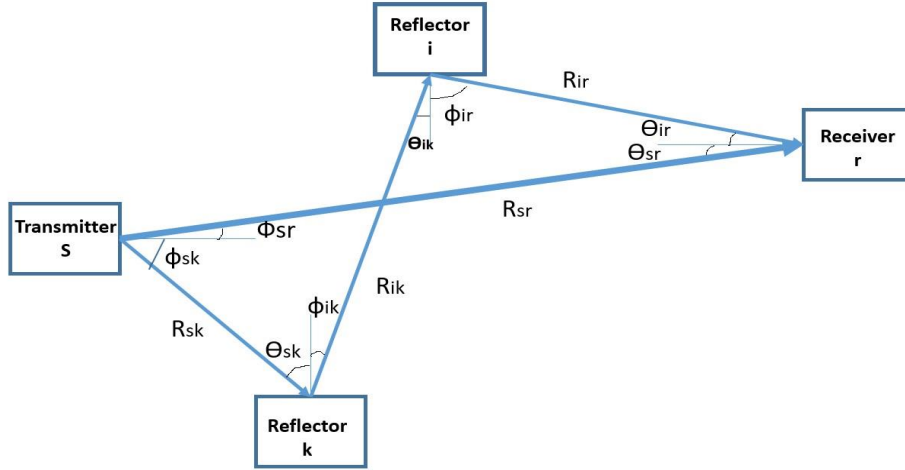


Fig. 3. Emitting and incident angles and other related parameters.

### 2.3. Polarization

When an optical signal is reflected on a solid surface, the amplitude or phase of the reflected light wave will be modified by the reflector. In general, the light wave which is an electromagnetic (EM) wave travels in the positive direction along the z-axis with regard to time. Its polarization will be perpendicular to the direction of propagation (in the x-y plane). In a noncoherent light source such as the LED, the polarization will be arbitrarily varied in the x-y plane.

Once incident upon a foreign media, the direction of polarization changes. This effect can be described by an  $N$  by  $N$  matrix,  $P_{N \times N}$ ,

$$P_{N \times N} = \begin{bmatrix} p_{11} & p_{12} & \dots & p_{1N} \\ p_{21} & p_{22} & \dots & p_{2N} \\ \dots & \vdots & \ddots & \vdots \\ p_{N1} & p_{N2} & \dots & p_{NN} \end{bmatrix}$$

According to the Malus law,  $p_{ij} = \cos^2(\alpha_{ij})$  and  $\alpha_{ij}$  is the transmission axis rotation angle [15].

### 2.4. Receiver Profile: $G_{N \times M}$

The transfer function between the reflectors and the receiver  $G_{N \times M}$  is an  $N$  by  $M$  matrix. It is represented as [9]:

$$G_{N \times M} = \begin{bmatrix} g_{11} & g_{12} & \dots & g_{1M} \\ g_{21} & g_{22} & \dots & g_{2M} \\ \dots & \vdots & \ddots & \vdots \\ g_{N1} & g_{N2} & \dots & g_{NM} \end{bmatrix}$$

The entry  $g_{ir}$  is the transfer function from element  $i$  to receiver  $r$ . It can be given by [9]:

$$g_{ir} = \frac{\rho_i \cos(\phi_{ir}) \cos(\theta_{ir}) A_r}{\pi R_{ir}^2} \delta\left(t - \frac{R_{ir}}{c}\right) u(FOV_r - \theta_{ir}) \quad (2)$$

where  $\phi_{ir}$  is the emitting angle from the element  $i$  to receiver  $r$ ,  $\theta_{ir}$  is the incident angle from the element  $i$  to receiver  $r$ ,  $R_{ir}$  is the distance between element  $i$  and receiver  $r$ ,  $A_r$  is the area of the receiver and  $FOV_r$  is the field of view of the receiver  $r$ .

## 2.5. Direct Response Matrix: $D_{J \times M}$

The direct (LOS) matrix  $D_{J \times M}$  is a  $J$  by  $M$  matrix. It is represented as:

$$D_{J \times M} = \begin{bmatrix} d_{11} & d_{12} & \dots & d_{1M} \\ d_{21} & d_{22} & \dots & d_{2M} \\ \dots & \vdots & \ddots & \vdots \\ d_{J1} & d_{J2} & \dots & d_{JM} \end{bmatrix}$$

The entry  $d_{sr}$  is the transfer function from the source  $s$  to the receiver  $r$ . given as [9]:

$$d_{sr} = \frac{\left(\frac{n+1}{2\pi}\right) \cos^n(\phi_{sr}) \cos(\theta_{sr}) A_r}{R_{sr}^2} \delta\left(t - \frac{R_{sr}}{c}\right) u(FOV_r - \theta_{sr}) \quad (3)$$

where  $n$  is the Lambertian order of the source,  $\phi_{sr}$  is the emitting angle from source  $s$  to receiver  $r$ ,  $\theta_{sr}$  is the incident angle from source  $s$  to receiver  $r$ ,  $R_{sr}$  is the distance between source  $s$  to receiver  $r$ .

## 2.6. Total Response Matrix: $H_{J \times M}$

The total impulse response matrix of the MIMO system, illustrated in Fig. 2, is given by:

$$H = D_{J \times M} + F_{J \times N} * ((\Phi_{N \times N})(P_{N \times N})) * G_{N \times M} \quad (4)$$

where  $*$  represents the convolution sign.

## 3. COMPLETE CHANNEL IMPULSE RESPONSE

Many factors can affect the V2V channel. V2V scenarios can be classified as large spatial scale (LSS), moderate spatial scale (MSS), and small spatial scale (SSS) depending on the transmitter-receiver distance. Due to the unique feature of V2V environments, the vehicular traffic density (VTD) also significantly affects the channel statistics, especially for MSS and SSS scenarios. In general, as the Tx-Rx distance decreases, the VTD impact increases. Directions of motion of the transmitter and receiver also affect channel statistics. The double-directional time-variant complex impulse response of a V2V channel can be modeled as the superposition of  $L$  resolvable paths or taps, where  $L$  is the total number of paths including the direct path,

$$h(t, \tau, \Omega_T - \Omega_R) = \sum_{l=1}^L h_l(t) \delta(\tau - \tau_l(t)) \delta(\Omega_T - \Omega_{lT}(t)) \delta(\Omega_R - \Omega_{lR}(t)) \quad (5)$$

where  $\tau_l(t)$ ,  $\Omega_{lT}(t)$ ,  $\Omega_{lR}(t)$  represents the excess delay, direction of departure (DoD) and direction of arrival (DoA) of the  $l^{\text{th}}$  resolvable path at time  $t$ , respectively,  $h_l(t)$  denotes the complex fading envelope of the  $l^{\text{th}}$  resolvable path and can be calculated from Eq. (6). The expected formula for the impulse response will be in the form [16]:

$$h_l(t) \sum_{i=1}^L a_i(t) e^{j\theta_{Ti}(t)} e^{j\theta_{Ri}(t)} \quad (6)$$

where  $\theta_{Ti}(t)$  and  $\theta_{Ri}(t)$  denote the DoD and DoA of the  $l^{\text{th}}$  path, respectively;  $a_i(t)$  is the complex envelope.

## 4. SIGNAL TRANSMISSION AND DETECTION

The optical wireless communication system over a multipath scattering channel is shown in Fig. 4. Here we consider a simple On-Off Keying scheme because our main objective is to evaluate the multipath channel model we just derived.

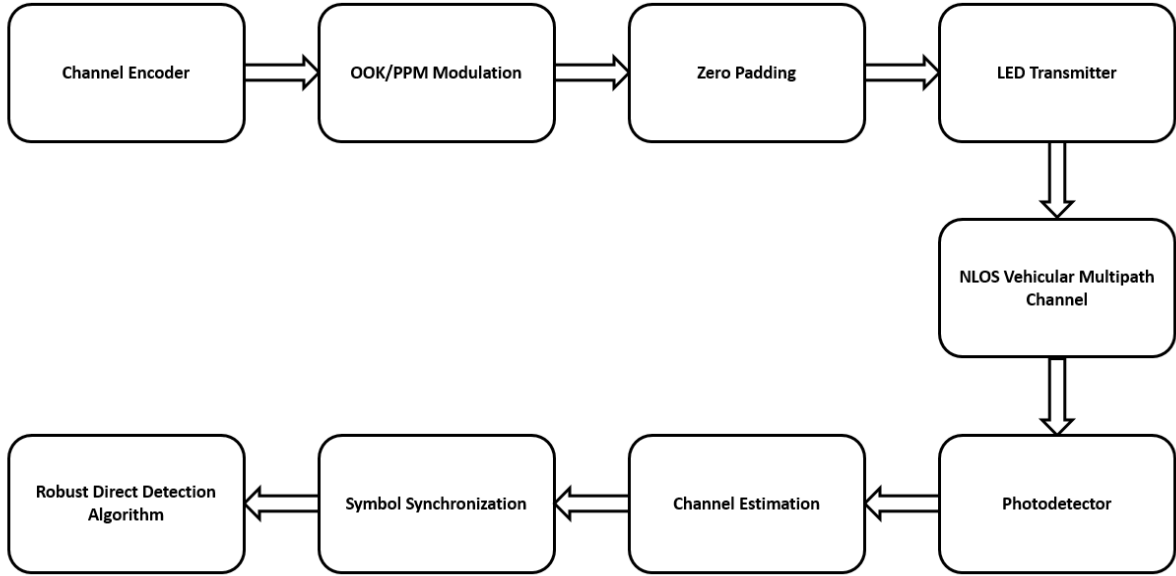


Fig. 4. The non-line-of-sight (NLOS) optical wireless scattering communication.

#### 4.1. Mitigating Channel Multipath Effects at the Transmitter

In order to mitigate multipath effects, we propose a zero padding (ZP) scheme for each data symbol with a guard interval which corresponds to the maximum path delay [17]. When the ZP technique is applied, a guard interval is appended prior to the transmission of individual symbols as illustrated in Fig. 5. The proposed ZP algorithm is based on the following operations that apply the previously derived channel transfer matrices in sections 2.1 - 2.5. The total time taken by the signal to travel from the transmitter to the receiver, via reflectors is considered for setting the symbol guard interval. Since it's a time varying environment, the guard interval is conditioned on the element's and scatterer's respective time delays and their variations.

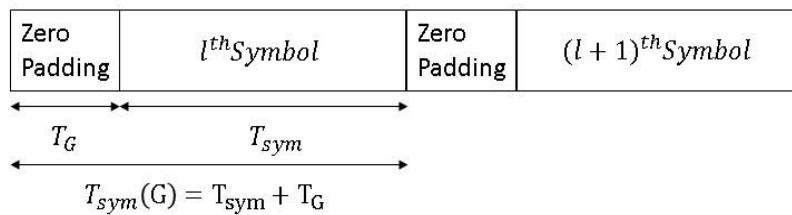


Fig. 5. Schematics of guard and symbol periods with ZP.

Let  $\tau$  be the path delay

$$\tau = \frac{R}{c} T_G = \max \begin{cases} \tau_{s,k} | \min\{F_{J \times N}\} \\ \tau_{i,k} | \min\{\Psi_{N \times N}\} \\ \tau_{i,r} | \min\{G_{N \times M}\} \\ \tau_{s,r} | \min\{D_{J \times M}\} \end{cases} \quad (7)$$

where  $T_G$ ,  $R$  and  $c$  are the guard period, distance and speed of light, respectively. The guard period  $T_G$  must be selected accounting for the maximum path delay over all path elements. Although ZP is generally considered as a bandwidth deficient schemes in a VLC environment, it's unlikely to hinder system performance.

## 4.2. Direct Detection

Direct Detection of the OOK modulated VLC signal can be done through the use of a photodetector. The output signals of the photo detector at the receiver considering the multipath channel can be given by

$$y(\tau) = \sum_{l=1}^L h_l(t)x(\tau - lT) + n(\tau) \quad (8)$$

where  $X(t) = [x_1(t), x_2(t), \dots, x_n(t)]$  is the data vector,  $T$  is the symbol interval and  $n(\tau)$  is the background radiation intensity. We may assume the channel and its respective multipath scatterers exhibit a standard Gaussian distribution. Hence, assuming a field effect transistor (FET) receiver, the noise variance at the photo detector can be given as follows [18]:

$$\sigma_{PD}^2 = \sigma_{shot}^2 + \sigma_{thermal}^2 \quad (9)$$

where

$$\sigma_{shot}^2 = 2q\gamma P_{rSignal}B + 2q\gamma P_{bg}I_2B \quad (10)$$

Here  $q$  is the electron charge,  $B$  is the noise equivalent bandwidth,  $P_{rSignal}$  is the received signal power,  $P_{bg}$  is the background radiation power,  $\gamma$  is a semi-empirical constant that depends on the carrier concentration in the channel and the device geometry, and  $I_2$  is the noise bandwidth factor that accounts for a rectangular transmitted pulse shape. The thermal noise variance is provided as [19]:

$$\sigma_{thermal}^2 = \frac{8pkT_A}{G}\eta AI_2B^2 + \frac{16p^2kT_A\Gamma}{g_m}\eta^2 A^2 I_3B^3 \quad (11)$$

where  $T_A$  is the environmental temperature,  $k$  is the Boltzman constant,  $p$  is the incident power,  $A$  is the receiver area,  $G$  is the open-loop voltage gain of the receiver amplifier,  $\eta$  is the capacitance of the photo detector per unit area,  $\Gamma$  is the FET channel noise factor,  $g_m$  is the FET transconductance and  $I_3$  is the noise bandwidth factor.

Since the Doppler shift will not exist in intensity modulation schemes, there is no need for a Doppler frequency compensator. With respect to receiving an OOK modulated symbol, direct detection will be applied by observing the minimized Euclidean distance from the average received signal power. Assuming channel state information (CSI) is known, a decision threshold will be derived as follows:

$$\eta_0 = E[y(\tau)] = E[\sum_{l=0}^L h_l(t)x_0(\tau - lT) + n(\tau)] \quad (12)$$

$$\eta_1 = E[y(\tau)] = E[\sum_{l=0}^L h_l(t)x_1(\tau - lT) + n(\tau)] \quad (13)$$

The Euclidean distance can be minimized as follows corresponding to an ideal single dimensional constellation:

$$\gamma = \min\{ || V_{rec.} - V_{exp.} || \} \quad (14)$$

where  $V_{rec.}$  is the instantaneous received signal represented by a vector and  $V_{exp.}$  represents the vector corresponding to the expected value following the OOK format. Hence, the optimum region will occur with a minimum Euclidean distance. Assuming the signals scattering are Gaussian distributed and it can be regarded as a plane wave, the following probability density function (PDF) can be stated with respect to the corresponding OOK designations represented as  $\gamma$ .

$$p(y|x_\gamma) = \frac{1}{\sqrt{2\pi(\sigma_{AWGN}^2 + \sigma_{PD}^2)}} \exp\left(-\frac{\|y - \eta_\gamma\|^2}{2(\sigma_{AWGN}^2 + \sigma_{PD}^2)}\right) \quad (15)$$

where  $\sigma_{AWGN}^2$  is the variance of the additive white Gaussian noise (AWGN).

In order to determine an approximate value for the decision threshold, the respective signal power for OOK is averaged and its Euclidean distance is conditioned at the receiver.

$$\alpha = \frac{[\eta_0 + \eta_1]}{2} \quad (16)$$

Equivalently, the decision threshold will be effectively decided by implementing the previously derived PDF. Taking into account the received signal phase errors, we can clearly see that as long as there are no substantial multipath artifacts, the decision region can be effectively implemented as follows:

$$\hat{y} = \begin{cases} p(y|x_0) > p(y|x_1) & y \approx 0 \\ p(y|x_0) < p(y|x_1) & y \approx 1 \end{cases} \quad (17)$$

## 5. SIMULATIONS

In our simulation, we use the ML toolbox in the Matlab (R2020b) suit of software. Our simulation parameters are shown in Table 1. Fig. 6 displays the overall 'Source to Receiver' path gains in a standard V2V scenario with respect to the emitted and received angles. Since the path gain depends on the emitted and received angles, a total window of  $-90$  to  $90$  degrees has been used in our simulation. A FOV of  $60$  degrees and a reflection coefficient of  $0.8$  have been applied. The transmitter element and received areas are considered to be approximately  $10^{-4} m^2$ . The final distance parameter is distributed between  $20$  m and  $120$  m. Note that an increase in the distance affects the slope of the overall distribution while the maximum peak remaining constant. Hence, Fig. 6 illustrates that the path loss is minimal when there is a direct LOS at a close distance, in which case the maximum SNR is also achieved.

Table 1. Geometry parameters and its simulation values.

Symbol	Description	Value
$s, r, i$ and $k$	Transmitter, receiver, and reflectors	(1-2), (0-6)
$\phi_{sr}$	Emitting angle from $s$ to $r$	$30^\circ$
$\theta_{sr}$	Incident angle from $s$ to $r$	$45^\circ$
$R_{sr}$	Distance between $s$ and $r$	$20-120$ m
$A_r$	Effective area of $r$	$1 \times 10^{-4} m^2$
$FOV_r$	FOV of $r$ with respect to $s$	$60^\circ$
$\phi_{sk}$	Emitting angle between $s$ and $k$	$-90^\circ - 90^\circ$
$\theta_{sk}$	Incident angle between $s$ and $k$	$-90^\circ - 90^\circ$
$A_k$	Reflector area	$150 cm^2$
$\rho_i$	the reflectivity	$0.8$
$\phi_{ir}$	Emitting angle between $r$ and $i$	$-90^\circ - 90^\circ$
$\theta_{ir}$	Incident angle from $i$ to $r$	$-90^\circ - 90^\circ$
$R_{sk}$	Distance between $s$ and $k$	$20-80$ m
$R_{ik}$	Distance between $i$ and $k$	$20-80$ m
$R_{ir}$	Distance between $i$ and $r$	$20-80$ m
$\phi_{ki}$	Emitting angle between $k$ and $i$	$-90^\circ - 90^\circ$
$\theta_{ki}$	Incident angle between $k$ and $i$	$-90^\circ - 90^\circ$
$I_s(a_s, \beta_s)$	Luminous intensity of $T$	$1040 cd$
$(a_s, \beta_s)$	Position angles of $T$	$-10^\circ, 10^\circ$

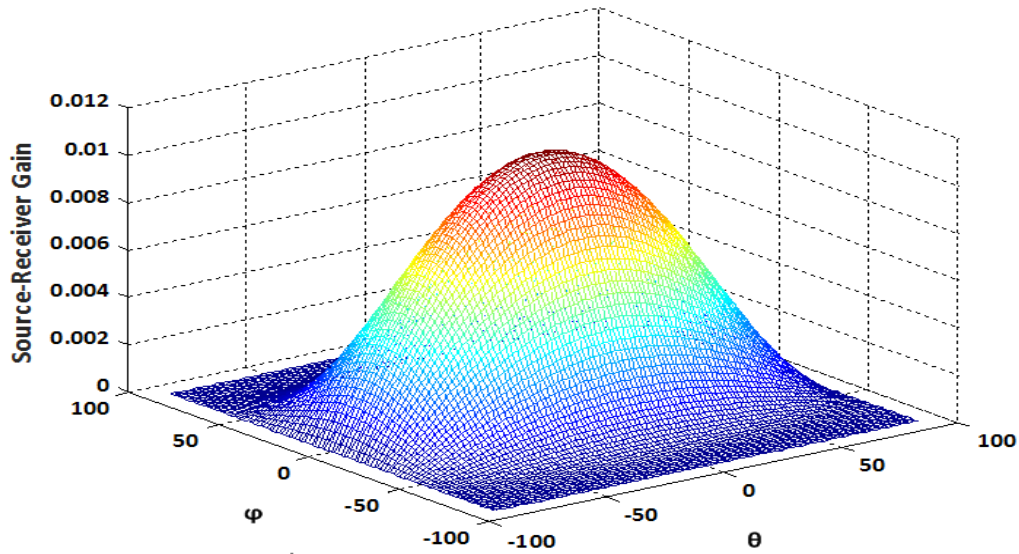


Fig. 6. Source to receiver transfer function.

Fig. 7 displays the multipath fading with varying path delays which shows greater fading as the path delay increases due to rapid fluctuations of the amplitude and phase. This is partly caused by the possibility of the transmitter and receiver being obstructed by a dense section thereby causing secondary interfering waves. In addition, an increased time delay amplifies scattering effects due to rough surfaces whose dimensions are on the order of the visible spectrum wavelength causing spreading.

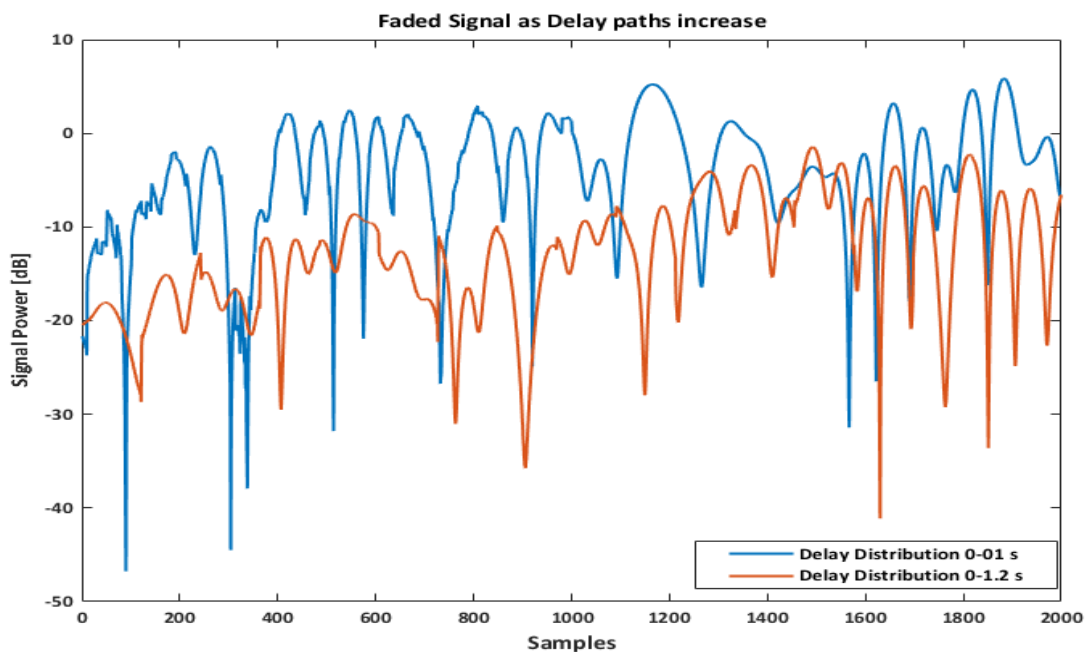


Fig. 7. Signal fading with varying multipath delays.

In Fig. 8, the BER for our proposed model was simulated by differentiating the normalized projected path distributions which is effectively incorporated as stochastic scattering effects. Fig. 8 shows that the BER increases as the dominant LOS component

decreases. The NLOS fading model represents our model whereas the LOS fading represents the ideal case without any scattered signal.

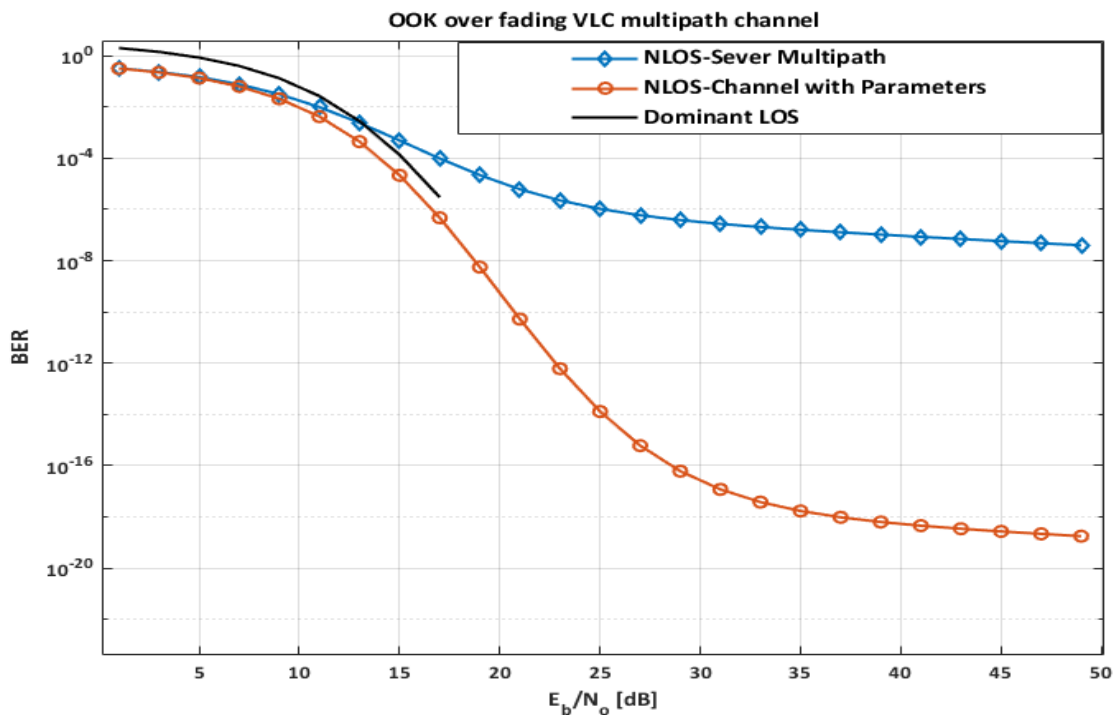


Fig. 8. Simulated BER with OOK and ML detection over VLC multipath channel.

## 6. CONCLUSIONS

For accurate evaluation of mobile V2V communication systems using VLC, an accurate channel model is essential. Developing such a channel model from the beginning is one of the objectives of this paper. General number of transmitting elements, reflectors and receiving elements are considered which essentially reflect a multipath MIMO optical wireless channel. The complete channel impulse response is derived by convolving the transmitter, channel and receiver matrices. This impulse response function is used to evaluate the channel, its dependency on the transmitter/receiver FOV and its fading characteristics. After the accurate channel model is derived, further investigation is done using a generic OOK communication system over this channel. Since the maximum channel delay can be estimated according to the proposed model, a ZP technique can be used for mitigating multipath effects. An expression for the PDF at the receiver is derived considering multipath effects as well as background radiation noise. Symbol detection at the receiver is done by minimizing Euclidean distance at the receiver.

## REFERENCES

- [1] P. Zhao, N. Chi, "3.2 gbps underwater visible light communication system utilizing dual-branch multi-layer perceptron based post-equalizer," *Optics Communications*, vol. 460, pp. 125197, 2020.
- [2] N. Chi, Y. Zhou, S. Liang, F. Wang, J. Li, Y. Wang, "Enabling technologies for high-speed visible light communication employing cap modulation," *Journal of Lightwave Technology*, vol. 36, no. 2, pp. 510-518, 2018.

- [3] P. Haigh, F. Bausi, Z. Ghassemlooy, I. Papakonstantinou, H. Le Minh, C. Fléchon, F. Cacialli, "Visible light communications: real time 10 Mb/s link with a low bandwidth polymer light-emitting diode," *Optics Express*, vol. 22, no. 3, pp. 2830-2838, 2014.
- [4] World Health Organization, *Supporting A Decade of Action*, WHO Global Status Report on Road Safety, 2021.
- [5] Q. Fu, D. Jin, J. Zhan, S. Zhang, Y. Li, Y. Liu, Z. Tao, L. Han, H. Jiang, "Study of multispectral polarization visible light propagation properties under smog conditions," in *2017 16th International Conference on Optical Communications and Networks*, pp. 1-3, 2017.
- [6] J. Armstrong, Y. Sekercioglu, A. Neild, "Visible light positioning: a roadmap for international standardization," *IEEE Communications Magazine*, vol. 51, no. 12, pp. 68-73, 2013.
- [7] S. You, S. Chang, H. Lin, H. Tsai., "Visible light communications for scooter safety," in *Proceeding of the 11th Annual International Conference on Mobile Systems, Applications, and Services*, pp. 509-510, 2013.
- [8] A. Skarmeta, P. Fernandez Ruiz, F. Bernal Hidalgo, J. Santa Lozano, *Deploying ITS Scenarios Providing Security and Mobility Services Based on IEEE 802.11 p Technology*, Vehicular Technologies - Deployment and Applications, InTech Open, 2013.
- [9] X. Fernando, H. Farahneh, *Visible Light Communications*, IOP Publishing, 2019.
- [10] A. Zekry, "Hybrid modulation schemes for data transmission improvement of indoor visible light communication system," *International Journal of Engineering and Technology*, vol. 7, pp. 2822-2829, 2018.
- [11] H. Farahneh, F. Hussian, X. Fernando, "De-noising scheme for vlc-based v2v systems; a machine learning approach," *Procedia Computer Science*, vol. 171, pp. 2167-2176, 2020,.
- [12] K. Siddiqi, A. Raza, S. Muhammad, "Visible light communication for v2v intelligent transport system," in *2016 International Conference on Broadband Communications for Next Generation Networks and Multimedia Applications*, pp. 1-4, 2016.
- [13] R. Netsianda, K. Ouahada, A. Ndjiougue, "A comparative study of different modulations for visible light communications," *University of Johannesburg Institutional Repository*, 2017.
- [14] Y. Alqudah, M. Kavehrad, "MIMO characterization of indoor wireless optical link using a diffuse-transmission configuration," *IEEE Transactions on Communications*, vol. 51, no. 2, pp. 1154-1160, 2003.
- [15] Y. Wang, C. Yang, Y. Wang, N. Chi, "Gigabit polarization division multiplexing in visible light communication," *Optics Letters*, vol. 39, no. 7, pp. 1823-1826, 2014.
- [16] C. Chen, D. Basnayaka, H. Haas, "Non-line-of-sight channel impulse response characterisation in visible light communications," in *2016 IEEE International Conference on Communications*, pp. 1-6, 2016.
- [17] P. Gawande, S. Ladhake, "Ber performance of ofdm system with cyclic prefix and zero padding," in *18th Asia-Pacific Conference on Communications*, vol. 6, no. 1, pp. 316-324, 2013.
- [18] S. Lee, S. Jung, "A SNR analysis of the visible light channel environment for visible light communication," in *18th Asia-Pacific Conference on Communications*, pp. 709-712, 2012.
- [19] R. Kapusta, H. Zhu, C. Lyden, "Sampling circuits that break the kt/c thermal noise limit," *IEEE Journal of Solid-State Circuits*, vol. 49, no. 8, pp. 1694-1701, 2014.